Rock Mechanics
and Rock Engineering 18, 1—15 (1985)

**Rock Mechanics
and Rock Engineering**

Analyses of Disking Phenomenon and Stress Field in the Region of an Underground Powerhouse

By

Weishen Zhu, Guangyu Li, and **Kejun Wang**

Institute of Rock and Soil Mechanics, Academia Sinica, Wuhan, China

Summary

The large underground power chambers of Ertan Hydropower Station will be built near the abutment on the left bank in a region with high initial stresses. In this paper, a statistical analysis is presented for the phenomenon of core disking in the dam site. On the basis of a number of stress measurements, the region of the river valley could be divided into three different geostress zones. It is shown that there exists a rather high horizontal stress of up to 30 MPa, and even over 60 MPa at the bottom of the river bed. A least square method has been introduced to get a continuous field of stress, which approximates the variable measured stress data.

Fig. 1. The location of Ertan dam site

1. Introduction

The Ertan Hydropower Station will be located in the remote mountain and gorge region of the Yalong River in southwest China (Fig. 1). The strata at dam region are Permian basalt (β) and deuterogenously intrusive syenite (ξ). The syenite mass with a length of about six km and a width of one km

extends northeastwards, and the dam site is located at the southwest end of the mass. The left bank is mainly composed of syenite while the right one is mainly composed of basalt. Both masses are rather intact and hard, the number and the dimensions of the faults in the masses are small. In syenite, there exist three main joint sets with strikes of NE 30—50°, NW 40—50° and NW 60°—NE 60°, the former two are more frequent. Along the bank of the dam site high mountains (about 400—500 m) with an average slope of 30—40 degrees are situated. The height of the dam

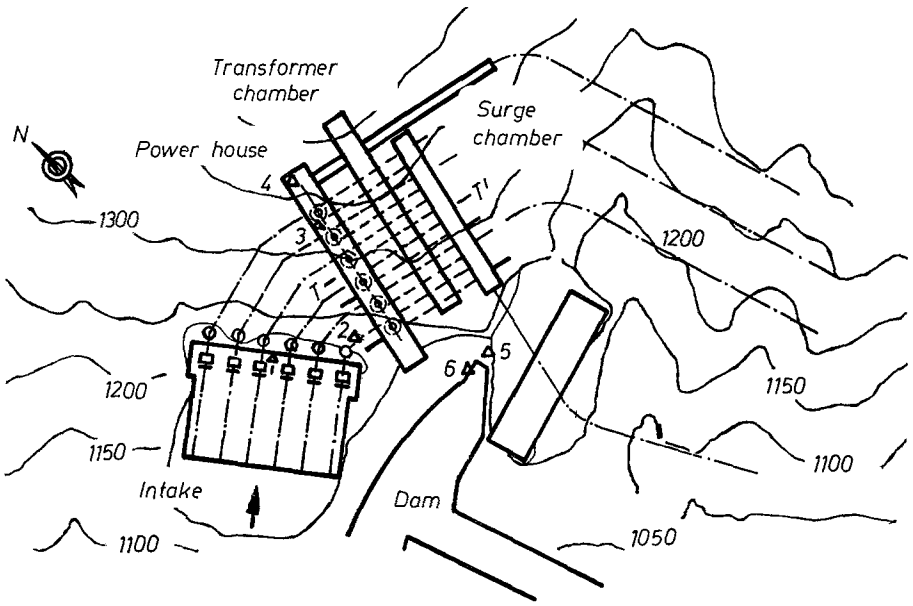

Fig. 2. Layout of underground power chambers at dam site

and the storage capacity of the reservoir are 245 m and 5.8×10^9 m^3 respectively. The installed capacity of the station is 3—3.5 GW. The underground power house with a length of 240 m, a width of 27.5 m and a height of 65 m will probably be built near the abutment on the left bank (Fig. 2). The feasibility of building this project is under consideration.

2. Rock Fracture Phenomena and Statistical Analysis

During the exploration stage of the project, nearly 200 prospecting bore-holes with a total length of over 20,000 m were drilled in order to make engineering geology conditions clear. In 84 bore-holes, phenomena of disking fracture of cores occurred, 45 holes of them are situated in the lower parts of the river bed and the valley slope.

The fracture surfaces are generally perpendicular to the axes of the bore-holes. Rupture phenomena took place locally at various depths in every

bore-hole. The average length of these stretches was about 0.2—0.5 m, but the longest stretch (in which 500 disks formed in succession) had a total length of up to 13.50 m (Fig. 3). Fracture surfaces are often fresh and rough.

Fig. 3

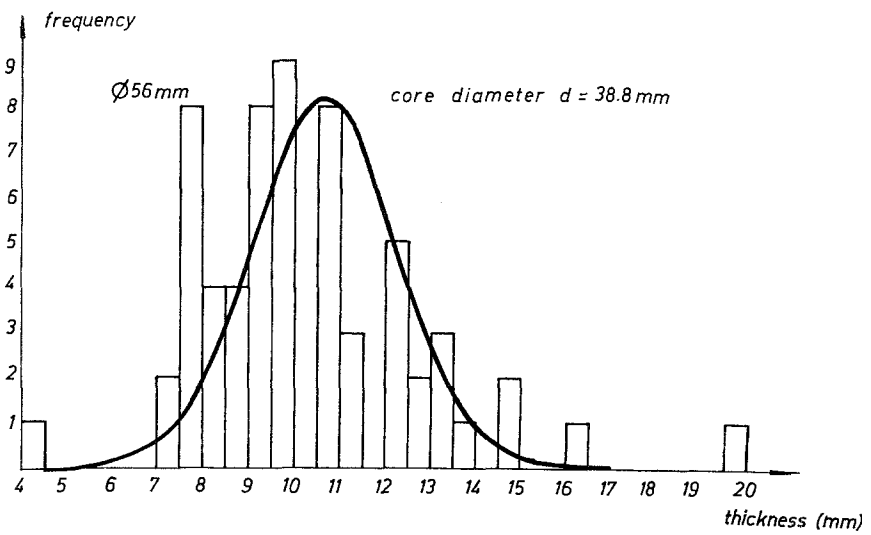

Fig. 4. Probability distribution of disk thickness for bits of ⌀ 56 mm

The top surfaces of the disks are concave and the bottom ones are convex, their thicknesses h are generally proportional to their diameters d ($h/d=$ 1/3—1/4).

Figs. 4 and 5 show the distribution of disk thicknesses for two different bore-hole diameters. The average thickness h is proportional to the core diameter d, in fact, the average thicknesses for the ⌀ 56 mm and ⌀ 108 mm bore-holes are 10.7 mm ($h/d=0.27$) and 20.9 mm ($h/d=0.25$) respectively.

The statistical distribution of 332 fracture bands of 54 bore-holes at the bottom of the valley is shown in Fig. 6. Higher fracture probability occurs at the altitudes between 930—975 m making up 74.7% of the total number. This band is 20—40 m just underneath the surface of the rock base. Ac-

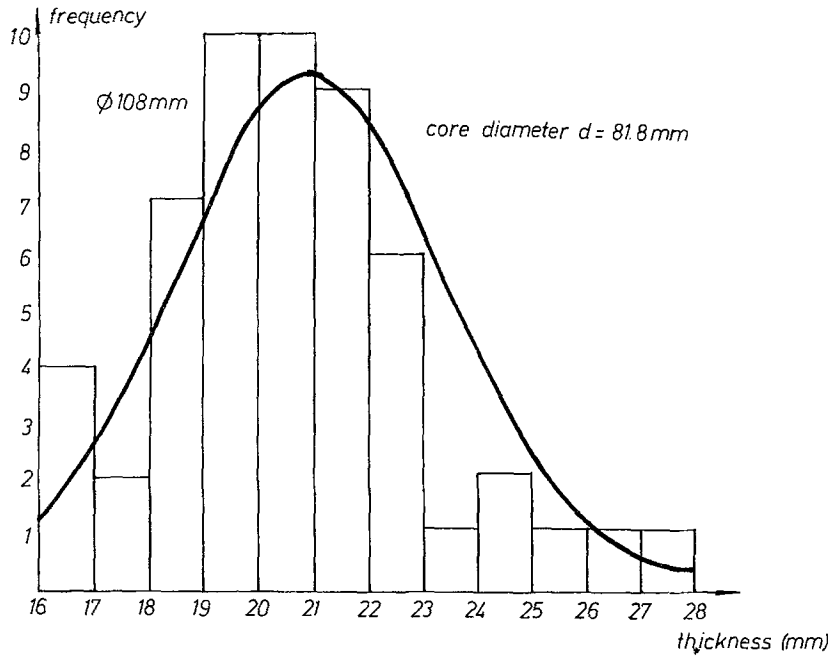

Fig. 5. Probability distribution of disk thickness for bits of ⌀ 108 mm

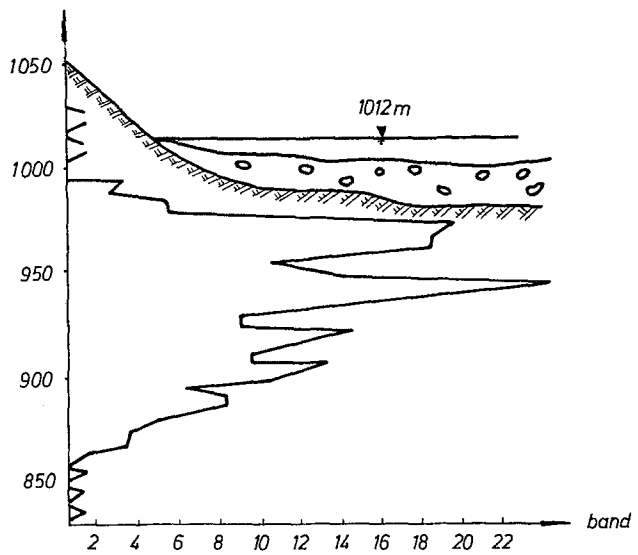

Fig. 6. Distribution of fracture bands along the altitude of the valley

cording to the results of a series of experiments and analyses, it may be said that the main contributing factors to disking phenomena are the stress concentration at the bottoms of the cores and partial unloading during drill process in a highly stressed region rather than other factors such as tectonic (joints), primary (stratifications, cleavages etc.) or the mechanical disturbance of the coring bits.

Statistical analysis has also shown that disking mainly occurred in syenite (amounting to 80% of the number of the whole bands). Therefore, a series of laboratory tests for syenite samples has been performed on a servo-controlled rigid machine; almost all syenite samples produced intensive burst

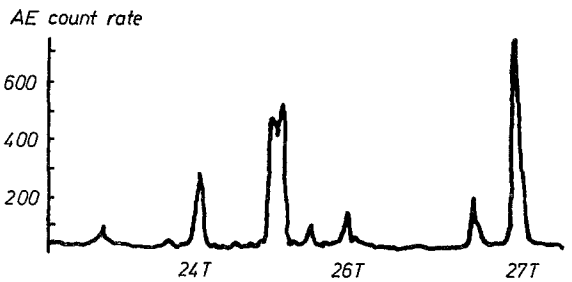

Fig. 7. Count rate of AE for dry samples under loading

sounds with flying out broken pieces when failure occurred. These tests were monitored by acoustic emission techniques, the AE frequency curve is shown in Fig. 7. The sudden character of AE occurring during loading is a good evidence of the outstanding brittleness of the rock.

3. Initial Stress in Rock Mass

The project is located in Gonghe Fault Block situated on the west side of the middle segment of Sichuan Yunan Tectonic Zone with a S-N strike and is surrounded by the deep and large-scale fracture zones of Xifantian and Jingqinghe, by the Yalon River and by the blind tectonic zone of Huaping Dukou with a strike of W-E. These fault zones had long activity in geological history, differential tectonic movements and strong seismic centres occurred along them. Around this region, there are some active fracture zones of Anning River (formed about 1600—1300 years from now), Jingqing (where an earthquake measured $M=6.7$ took place in 1467), Xigeda (1000 years ago). Weak earthquakes frequently occurred in recent time in this geologically active region. The Gonghe Fault Zone, where no intense earthquakes were recorded in history, is rather intact itself, and can be considered a relatively stable island in recent geological activity.

The dam site is located in the deeply cut valley of the Yalong River, which is oriented N 60^0 W. The valley is V shaped and asymmetrical: the left bank is higher and has an inclination of 25—40^0, whereas the right one has an inclination of 30—45^0.

The landform and the geological structure suggest that the dam site is located in a high stress region. High stress conditions can be predicted by both the phenomenon of core disking, which often occurred in prospection bore-holes (especially in those located in the river bed), and the phenomenon of rock burst, which took place sometimes in the exploration adits with direction parallel to the orientation of the river.

In order to determine the initial stress in the rock mass, a great number of in-situ tests were performed using overcoring techniques. About 700 original data have been obtained from 45 bore-holes with a total length of 460 m. Three different probes and instruments were used for the tests as indicated in the following:

1) Bore-hole Deformeter

It consists of four steel ring transducers by which the radial deformations along four directions at 45 degrees from each other can be measured

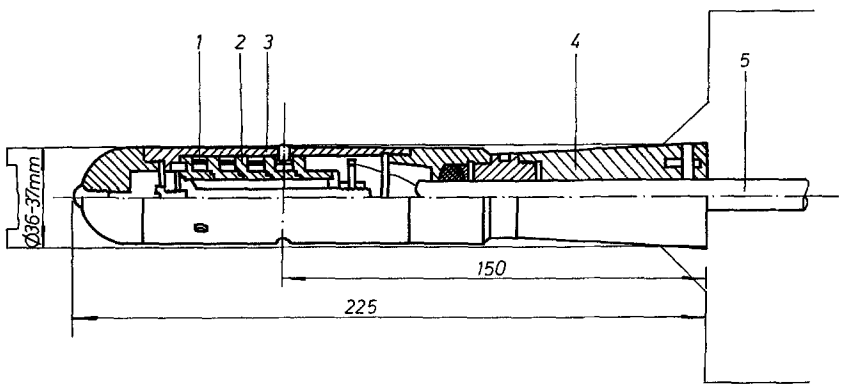

Fig. 8. Longitudinal section of the borehole deformeter
1 — Steel; 2 — Frame; 3 — Shell; 4 — Conical stopper; 5 — Cable

simultaneously (Fig. 8). When the deformeter is equipped with strain gauges of 1 $\mu\varepsilon$ sensitivity, its range of measurement and sensitivity are 0.8 mm and 0.0001 mm respectively. The calibration accuracy is 0.5%. Because the accu-

Table 1. *Comparison Between Preloading Stress and Measured Stress*

Type of rock	Dimension of specimen (cm)	State of loading	Preloading stress (MPa)			Measured stress (MPa)		
			σ_1	σ_2	φ	σ_1	σ_2	φ
Granite	50×50×80	uniaxial	−5.2	0	0	−5.5	0.7	−7°
	50×50×80	uniaxial	0	0	0	0.3	0.9	/
	50×50×80	uniaxial	0	0	0	−0.2	0.4	/
Dolomitic	35×35×60	biaxial	−9.6	−4.6	0	−9.1	−4.8	−4°
Limestone	35×35×60	biaxial	−9.4	−4.9	0	−10.0	−4.1	−12°

φ is the angle between σ_1 and horizontal axis. Clockwise positive.

racy of stress measurement depends mainly upon the deformability of the rock, overcoring tests were performed on large size rock samples preloaded with uniaxial or biaxial stresses in order to determine the overall accuracy of the system (Table 1). Because the syenite and the basalt are less fractured and more deformable than the granite and limestone in which the tests of Table 1 were carried out, a better accuracy can be expected in the in-situ measurements.

2) Piezo-magnetic Strain Gauge

This gauge is somewhat similar to the Hast strain gauge of Sweden. The disadvantage of the bore-hole deformeter and Piezo-magnetic strain gauge is that three bore-holes must be drilled along different directions in order to measure the complete stress sensor at one point.

3) Triaxial Bore-hole Strain Gauge

Three sets of strain rosette having four strain gauges each are stuck on the bore-hole wall by means of a wedge mechanism, after hardening of the cement overcoring is effected. An obvious advantage of this probe, similar to that described by Leeman, is that only one bore-hole is needed for determining the complete stress.

For the three techniques mentioned above, always the same diameters for the central bore-hole (36 mm) and for the overcoring one (130 mm) were adopted.

The results of the tests are shown in Tables 2, 3, 4 and Fig. 9.

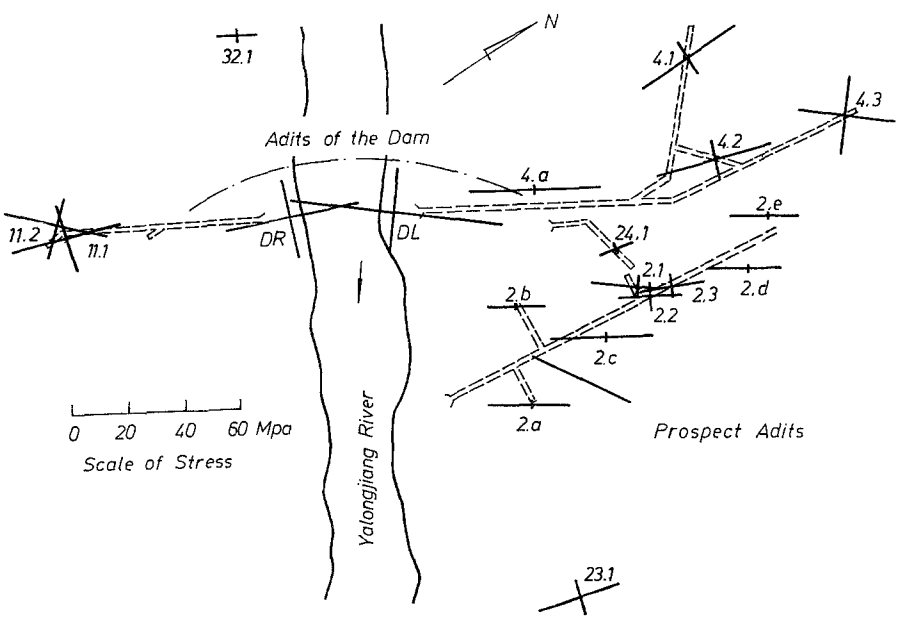

Fig. 9. Components of measured stresses in horizontal plane

The azimuth of the major principal stress of these twelve points is mainly about NE 30°, namely perpendicular to the direction of the river.

In order to obtain information about the influence of stress relief near the valley slopes, another six bore-holes were drilled along a direction parallel to the bank's direction in order to measure the plane stress state on a vertical section with a strike of NE 30° at different distances from the slope surface.

Table 2. *Measured Values of Complete Stress Components*

No. of meas. points*	Rock type	σ_1			σ_2			σ_3			Instruments
		MPa	α	β	MPa	α	β	MPa	α	β	
2.1	Syenite	25.5	34°	23°	8.8	140°	33°	2.4	277°	48°	(1)
2.2	do.	18.4	31°	45°	7.3	141°	19°	−1.9	245°	34°	(1)
2.3	do.	19.1	20°	57°	6.6	160°	27°	5.6	260°	18°	(2)
2.4	do.	23.0	35°	22°	15.7	115°	−20°	6.2	169°	56°	(3)
4.1	Altered syenite	29.0	359°	−8°	11.5	76°	57°	7.2	275°	32°	(2)
4.2	Basalt	37.6	22°	26°	17.0	111°	−3°	10.2	195°	63°	(2)
4.3	Syenite	25.1	39°	−7°	23.9	137°	−47°	10.9	123°	42°	(2)
24.1	do.	9.4	353°	31°	4.4	163°	58°	4.2	261°	4°	(2)
23.1	Agglomerate	26.1	16°	27°	16.5	101°	−10°	10.6	172°	61°	(2)
11.1	Basalt	29.7	11°	−24°	21.6	95°	12°	4.0	341°	63°	(1)
11.2	do.	31.9	48°	−8°	14.7	132°	26°	9.0	342°	63°	(3)
32.1	Syenite	10.7	28°	−24°	4.1	123°	−10°	1.4	54°	64°	(2)

* No. 2.1 means meas. point 1 in prospect adit 2.

α azimuth of stress (plus for clockwise, minus for counter-clockwise from north).

β dip angle of stress (plus for elevation).

Table 3. *Data of Measurements for Vertical Section of NE 30°*

No. of meas. points	Rock type	σ_1 (MPa)	σ_3 (MPa)	θ_1	Instrument
2. a	Syenite	24.0	2.8	31°	(1)
2. b	Syenite	16.6	1.7	46°	(1)
2. c	Syenite	30.8	10.3	29°	(1)
2. d	Syenite	19.3	2.0	26°	(1)
2. e	Syenite	20.6	4.9	46°	(1)
4. a	Syenite	39.6	4.5	43°	(1)

σ_1, σ_3 are max. and min. principal stresses for deep boreholes for specific section.

θ_1 is dip of σ_1 (plus for clockwise).

Two vertical bore-holes were drilled at the sides of the river so that the stress concentration at the bottom of the river could be determined, the measurements were performed during dry season while the drilling platform was erected above water. It is interesting to mention that at the depth of 37.5 m the rock cores (30 cm long) were fractured during overcoring into disks

Table 4. *Data of Measurements for Deep Boreholes at River Bed*

Location	Depth of meas. point	σ_1 (MPa)	σ_3 (MPa)	θ_1	Instrument
Left bank	17.6 m	1.8	0.5	NW 78°	(1)
Left bank	24.5 m	4.9	1.2	NE 87°	(1)
Left bank	30.0 m	17.6	2.9	NW 80°	(1)
Left bank	37.5 m*	63.7	28.5	NE 34°	(1)
Left bank	40.5 m	64.6	25.4	NE 50°	(1)
Left bank	45.0 m	48.4	19.8	NE 28°	(1)
Left bank	55.3 m	58.8	30.9		(1)
Left bank	59.4 m	59.8	31.3	NE 50°	(1)
Right bank	21.9 m	1.5	−1.0	NE 6°	(1)
Right bank	26.8 m	1.1	−2.0	NW 32°	(1)
Right bank	38.0 m	14.2	12.4		(1)
Right bank	45.0 m	38.6	23.8	NE 12°	(1)
Right bank	53.5 m	39.9	22.2	NE 32°	(1)
Av. value below 37.5 m of left bank		58.9	27.2	NE 40°	
Av. value below 45.0 m of right bank		39.2	23.2	NE 22°	

with an average thickness of 2.5 cm, some of them still partly stuck together (Fig. 10). In spite of this phenomenon, four sets of stress values were accurately obtained from four deformation curves owing to the excellent

Fig. 10

properties of Type 36-2 deformeter. These four sets of stress values can be checked with each other, the deviation is less than 5% (see the values marked with "*" in Table 4).

Notwithstanding the great number of stress measurements, the in-situ stress distribution is made uncertain by the variations in structure and lithology of the rock mass. Therefore, back analysis has been done using FEM to get the general stress field at the dam site (Bai and Li, 1982).

From the measured data and the FEM analysis the following conclusions were drawn:

— Field measurements have indicated that the dam site is located in a high stress region, for instance, the max. stresses in syenite reach 26 MPa (up to 40 MPa for some specific bore-holes) and those in basalts are even

higher (about 30—38 MPa). The highest stresses were measured in the river bed (60 MPa for left bank and 40 MPa for right bank). In addition, the differences between major and minor principal stresses are quite large. They are about 7—14 MPa at the two banks and even up to 20 MPa at the river bed. Instability of underground openings may occur during future excavation because the max. initial shear stress is close to the cohesion of the rock samples, which is about 20—30 MPa.

— The regional geological situation indicates a N-S orientation of the main tectonic stress and the solutions of earthquake focus mechanism show an orientation of actual tectonic major principal stress of about NW 10—20°. But at the site of the engineering project, the in-situ measurements have shown that the max. principal stress has an orientation of NE 30° (i. e. perpendicular to the strike of the river) and that its dip is slightly smaller than the slope of the bank. This eloquently points to the governing influence of the local morphological conditions in the river valley for the initial stress distribution.

— Measurements and calculations have shown that the rock mass may be divided into three zones — stress released zone, stress concentration zone and constant stress zone — each characterized by a different configuration of the initial stress (Fig. 11). The coefficient of stress concentration is about 1.5.

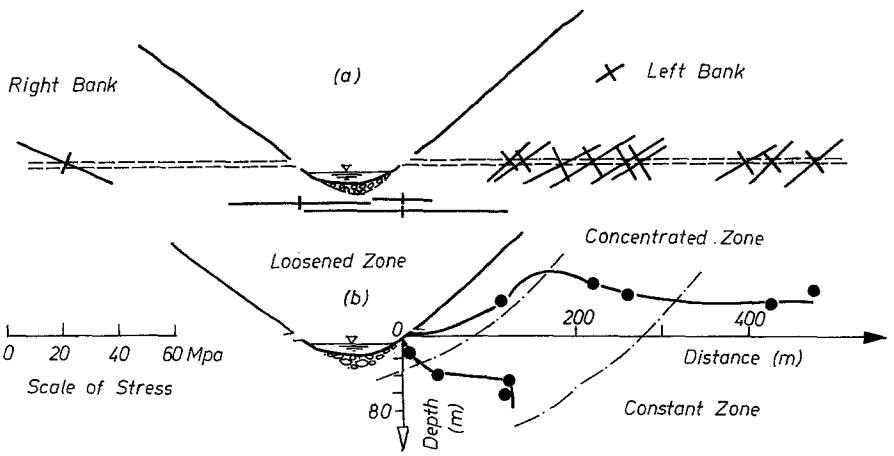

Fig. 11. a) Principal stresses in syenite in cross section of the river. b) Three stress zones characterized by measured stresses

The bottom of the river bed is in the region with most serious stress concentration and all the measurements performed in this part fell within this stress concentration zone. Its depth can be evaluated from the positions of disking bands appearing in bore-holes and from the FEM analysis; it is about 160 m (see Fig. 11).

— The accumulated strain energy is different from place to place owing to variable mechanical properties of rock, for instance, a rock mass with a high elastic modulus or triaxial strength can lead to a high stress concen-

tration. It can be seen from field measurements that the major principal stresses are 19—24 MPa for syenite and 29—34 MPa for basalt in constant stress zone.

— The ratio of the three principal stresses is about 1 : 0.5 : 0.25, their azimuths are NE 30°, NW 60°, NE 30°, and their trends and dips are SW 30°, horizontal (parallel to the river direction), and NE 60° respectively. In certain sites initial stresses deviate from normal values because of the effect of local tectonic alteration.

— The phenomena of disking occurring in vertical bore-holes at the river bed are clear evidences of the existence of high horizontal initial stress. The two principal stresses on the horizontal plane on which measurement was performed are 63 and 28 MPa respectively.

4. The Approximation of the Geostress Field by Least Square Method

It is quite possible that the underground chambers will be built near the abutment of the dam and the FEM should be employed to analyse the stability of the chambers. The geostress field in the bank region, as described in the previous section, is a variable one owing to the influences of the topography and of the different lithotypes characters. On the basis of the data obtained from stress measurements as well as the condition that some stress components are zero at the ground surface, a least square method was used to derive a continuous geostress field. The region where the calculation was effected (a huge roughly cubic rock mass of which the top surface is the natural ground surface) has the bottom at an elevation of 800 m, and its four vertical side walls at a distance of 200 m from the outer side-walls of the envisaged chambers.

4.1 Form of the Stress Functions and Conditions

The differential equilibrium equations may be written as follows.

$$\begin{aligned} \frac{\partial \sigma_x}{\partial x} + \frac{\partial \tau_{xy}}{\partial y} + \frac{\partial \tau_{xz}}{\partial z} &= 0 \\ \frac{\partial \tau_{yx}}{\partial x} + \frac{\partial \sigma_y}{\partial y} + \frac{\partial \tau_{yz}}{\partial z} &= 0 \\ \frac{\partial \tau_{zx}}{\partial x} + \frac{\partial \tau_{zy}}{\partial y} + \frac{\partial \sigma_z}{\partial z} - \varrho g &= 0 \end{aligned} \tag{1}$$

in which

ϱ — density of rock

g — gravitational acceleration.

Eqs. (1) are linear non-homogeneous of which the solution are superimposition of the general solutions of the corresponding homogeneous equations and the special solutions of the non-homogeneous equations. The special solutions are taken as:

$$\sigma_x = \sigma_y = \sigma_z = \tau_{xy} = \tau_{yz} = 0, \quad \tau_{zx} = \varrho g x.$$

Then the general solutions to the homogeneous equation corresponding to the system (1) can be described in terms of stress functions $\phi_1(x, y, z)$, $\phi_2(x, y, z)$, $\phi_3(x, y, z)$. Granted that the stress functions are in the form of the fourth order multinomials of coordinates (x, y, z), the components of stress must be the second order function of coordinates; as a result, they can be fitted to the variation of the initial stresses measured in situ. The general expression of stress function is

$$\begin{aligned}\phi_1 = {} & a_1x^2 + a_2y^2 + a_3z^2 + a_4xy + a_5yz + a_6zx + a_7x^3 + a_8y^3 \\ & + a_9z^3 + a_{10}xyz + a_{11}x^2y + a_{12}x^2z + a_{13}xy^2 + a_{14}y^2z + a_{15}z^2x \\ & + a_{17}yz^2 + a_{18}x^4 + a_{18}y^4 + a_{19}z^4 + a_{20}xy^3 + a_{21}xz^3 + a_{22}x^3y \\ & + a_{23}yz^3 + a_{24}x^3z + a_{25}y^3z + a_{26}x^2y^2 + a_{27}x^2z^2 + a_{28}y^2z^2 \\ & + a_{29}x^2yz + a_{30}y^2xz + a_{31}z^2xy.\end{aligned} \tag{2}$$

Similarly, we can get the function ϕ_2 and ϕ_3. Considering the following relations between stress functions and stress components:

$$\begin{aligned}\sigma_x &= \frac{\partial^2\phi_3}{\partial y^2} + \frac{\partial^2\phi_2}{\partial z^2} & \sigma_y &= \frac{\partial^2\phi_1}{\partial z^2} + \frac{\partial^2\phi_3}{\partial x^2} \\ \sigma_z &= \frac{\partial^2\phi_2}{\partial x^2} + \frac{\partial^2\phi_1}{\partial y^2} & \tau_{xy} &= -\frac{\partial^2\phi_3}{\partial x\,\partial y} \\ \tau_{yz} &= -\frac{\partial^2\phi_1}{\partial y\,\partial z} & \tau_{zx} &= -\frac{\partial^2\phi_2}{\partial z\,\partial x}\end{aligned} \tag{3}$$

The stress components can be expressed as follows:

$$\begin{aligned}\sigma_x = {} & b_0 + b_1x + b_2y + b_3z + b_4x^2 + b_5y^2 + b_6z^2 \\ & + b_1xy + b_8yz + b_9zx.\end{aligned} \tag{4}$$

Where

$$\begin{aligned} b_0 &= 2(a_2'' + a_3') & b_1 &= 2(a_{13}'' + a_{15}') \\ b_2 &= 2(3a_8'' + a_{16}') & b_3 &= 2(a_{14}'' + 3a_9') \\ b_4 &= 2(a_{26}'' + a_{27}') & b_5 &= 2(6a_{18}'' + a_{28}') \\ b_6 &= 2(a_{28}'' + 6a_{19}') & b^7 &= 2(3a_{20}'' + a_{31}') \\ b_8 &= 6(a_{25}'' + a_{23}') & b_9 &= 2(a_{30}'' + 3a_{21}')\end{aligned}$$

(a' and a'' are coefficients of ϕ_2 and ϕ_3).

Similar equations can be written for the other stress components. Substituting (3) into compatibility equations expressed in terms of stress components, namely,

$$(1+\nu)\,\nabla^2\sigma_x + \frac{\partial^2\Theta}{\partial x^2} = 0 \tag{5}$$

(the equations expressed in terms of σ_y, σ_z, τ_{xy}, τ_{yz}, τ_{zx} are not written for simplicity)

where

$$\Theta = \sigma_x + \sigma_y + \sigma_z$$

ν — poisson's ratio.

It is possible to eliminate six of interpolating coefficients of Eq. (4). The above stress components will satisfy the equilibrium and compatibility equations automatically.

4.2 The Processes of Approximation by Least Square Method

This process makes use of the boundary conditions at the topographic surface and of the stress values determined by means of the in-situ measurements. At a boundary point on the surface where the direction cosines of the outernormal are l, m, n, the normal and tangential tractions are equal to zero, namely,

$$\begin{aligned} X_\nu &= \sigma_x l + \tau_{xy} m + \tau_{xz} n = 0 \\ Y_\nu &= \tau_{yx} l + \sigma_y m + \tau_{yz} n = 0 \\ Z_\nu &= \tau_{zx} l + \tau_{zy} m + \sigma_z n = 0. \end{aligned} \tag{6}$$

The boundary conditions can be written in terms of interpolating coefficients if the stress components defined in terms of these coefficients (Eq. 4) are substituted into Eqs. (6).

In conclusion 6 equations are available for each point where the complete stress tensor has been determined and 3 equations can be written for each point selected on the topographic surface. The general form of these equations is

$$A_1 Q_1 (x_i) + A_2 Q_2 (x_i) + \ldots + A_n Q_n (x_i) = B_i \tag{7}$$

in which,

A_n — unknown interpolating coefficients ($n = 55$ are independent ones for this case);

X_i — coordinates of point (x, y, z);

Q_j — power functions of coordinates $(j = 1, 2, \ldots, n)$;

B_i — measured values $(\sigma_x, \sigma_y, \ldots)$, or zero values of tractions at the boundary points $i = 1, 2, \ldots, m$, $m = 6 \times I + 3 \times K$, I — the number of measuring points, K — the number of selected boundary points.

A least square method was applied to obtain the best estimates of the A_i coefficients. In Fig. 12 the stress values found in six measurement points are compared with the estimated given by least square method. A good coincidence can be noted except for individual components of certain specific points. The relative locations of the measurement points with respect to the underground chambers are illustrated in Fig. 2. The continuous stress

field of the chambers area was given with this approximation and the projection of the stress field in the middle section of the chambers was shown in Fig. 13, which was applied to two and three dimensional FEM analyses of the chambers.

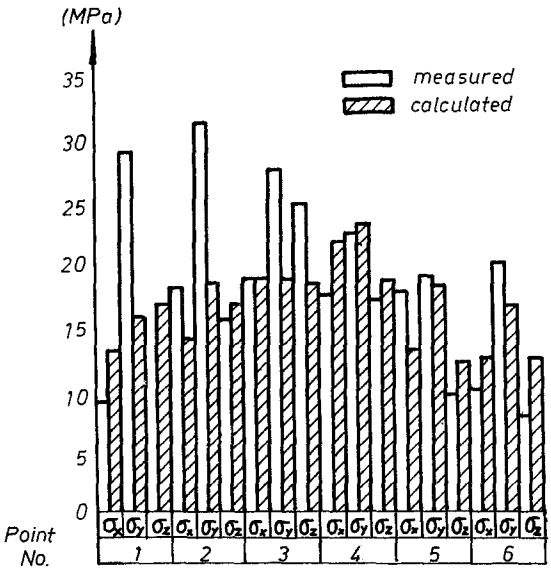

Fig. 12. Comparison of stress components between measured and calculated ones

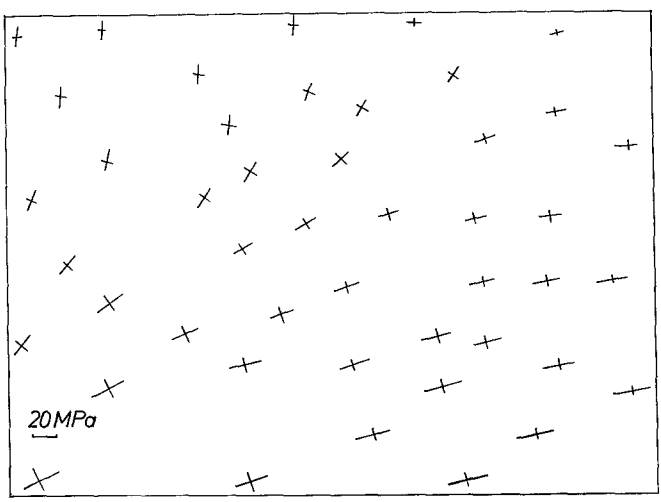

Fig. 13. Projection of stress field in the middle section of the chambers

5. Conclusions

— The phenomena of core disking frequently occurring in bore-holes at the dam site seem to result mainly from the rather high rock stresses and obvious brittleness of syenite in the region.

— A large number of measurement results indicates that the stress field around the project region is strongly affected by topography. The orientation of maximal principal stress is perpendicular to the river and its value, in general, is about 25—30 MPa, and the highest value at the river bed is over 60 MPa. The ratio of three principal stresses is 1 : 1/2 : 1/4. As to the distribution pattern of stress field, it can be classified into three zones, i. e., stress relaxation zone, stress concentration zone and stress stable zone.

— When the stress values measured in-situ indicate variations of the stress field, an approximate distribution of the stress field to be used in FEM analyses can be found by least square method.

Acknowledgements

Many data in-situ were offered by the Institute of Power Survey and Design, Chengdu. Assistance in translating this paper was given by Mr. Zhu Zouduo.

References

Bai, S., Li, G. (1982): Stress Measurement of Rock Mass in Situ and the Law of Stress Distribution in a Large Dam Site. Issues in Rock Mechanics, 23rd Symp. on Rock Mechanics, U. S. A.

Bai, S., Zhu, W., Wang, K. (1983): Some Rock Mechanics Problems Related to a Large Underground Power Station in a Region with High Rock Stresses. Proc., 5th Int. Congress on Rock Mechanics, Melbourne. D. 271, Australia.

Durelli, A. J., Obert, L., Parks, V. J. (1968): Stress Required to Initiate Core Disking. Trans SME, Vol. 241. Sept.

Hast, N. (1967): The State of Stresses in the Upper Parts of the Earth's Crust. Engineering Geology, *4* (no. 1).

Leeman, E. R. (1966): The Determination of the Complete State of Stress in Rock in a Single Borehole-Laboratory and Underground Measurements. C. S. I. R., Report. 538. Pretoria, South Africa.

Obert, L., Stephenson, D. E. (1965): Stress Conditions Under which Core Disking Occurs. Trans. SME, Vol. 232. Sept.

Shi, J. (1979): Brittle Fracture of Rock at High Stress Region. Interior Report of Inst. of Power Survey and Design, Chengdu.

Stacey, T. R. (1982): Contribution to the Mechanism of Core Disking. J. S. Afr. Inst. Min. Metall. *82* (no. 9).

Sugawara, K., Kameoka, Y., Saito, T., Oka, Y., Hiramatsu, Y. (1978): A Study on Core Discing of Rock. J. Min. Inst. of Japan *94*, 1089 (78—11).

Zhu, W., Wang, K., Peng, G. (1984): The Stability of Underground Power Chambers in Brittle Rock. Int. Conf. Case Histores in Geotechnical Engineering. St. Louis, MO, U. S. A.